Available online at www.sciencedirect.com
ScienceDirect
Journal of Power Sources 160 (2006) 1074–1087
JOURNAL OF POWER SOURCES
www.elsevier.com/locate/jpowsour

Thermal and electrochemical model of internal reforming solid oxide fuel cells with tubular geometry

D. Sánchez *, R. Chacartegui, A. Muñoz, T. Sánchez

Escuela Técnica Superior de Ingenieros de Sevilla, Camino de los Descubrimientos s/n, 41092 Sevilla, Spain

Received 11 November 2005; received in revised form 27 January 2006; accepted 21 February 2006
Available online 11 May 2006

Abstract

A two-dimensional axisymmetric model of a tubular solid oxide fuel cell (SOFC) is presented. The model analyzes electrochemistry and heat transfer inside the cell with new approaches to thermal and chemical simulations being introduced. For the reforming process a new approach based on traditional hypotheses, equilibrium and kinetic theory, is proposed. Thus, there is not a single assumption for the reaction but both situations are taken as possible depending on composition and temperature; results show that equilibrium is reached near the entry zone of the cell and the reaction is kinetically controlled later. Thermally, a rigorous study of radiative heat exchange between the anodic gas and the anode surface is included in order to evaluate its effect on global performance. Results show that this effect can be neglected in most cases but, under certain operating conditions, deviations of up to 1% may appear.

Additionally, other improvements have been done with respect to previous works: viscosity and electrical conductivity of gases depend on concentrations; evaluation of concentration losses includes a new description of binary diffusion coefficients; calculation of convective heat transfer coefficients includes thermal entry length and laminar/turbulent flow; heat generation in the inner part of the cell accounts for the heat release due to Joule effect.
© 2006 Elsevier B.V. All rights reserved.

Keywords: Solid oxide; Fuel cell; Reforming; Gas radiation

1. Introduction

The electric power generation system will undergo severe changes in the following decades. This transformation is aimed at improving the performance of power generators in three different ways: (i) more efficiency, (ii) lower emissions and (iii) proximity to final consumer.

Starting from the latest goal, proximity to consumer, it must be said that the current layout of the electric power transmission grid is highly inefficient in two ways. Nowadays, long distance transmission lines are used to connect power plants with load centres, what inevitable leads to electric losses as high as 7% of transmitted power. In addition, these transmission lines are coupled to high capacity power plants. When one of these plants is put out of service for some reason, generation and load are unbalanced and the situation may not be easy to sort out. For all these reasons, there is agreement between all partners of the electricity market to evolve at least partially towards a so called "distributed generation system", characterized by the integration of generators into consumers' environment. Thus, a new scenario is foreseen where rated power and emissions of generators lower while efficiency increases.

Along the twentieth century, maximum efficiency values between 50% and 60% (LHV based) have been achieved by fossil-fuel based power plants, with outputs ranging from 50 MW, diesel, to 800 MW, natural gas combined cycle. In spite of this, the efficiency of this kind of generators when applied to a distributed system is significantly lower than 50% due to the reduction in rated power. A new technology is needed and fuel cells are among the most promising options.

Fuel cells, particularly solid oxide fuel cells, are free of ozone destructive emissions as there is in principle no carbon monoxide or nitrogen oxide in the exhaust gas. In fact, only carbon dioxide and water steam are emitted, while traces (i.e. less than 1 ppm) of NO_x may be generated in residual combustion processes. These two species are greenhouse gases but the total amount

* Corresponding author. Tel.: +34 954 48 64 88; fax: +34 954 48 72 43.
E-mail address: davidsanchez@esi.us.es (D. Sánchez).

0378-7753/$ – see front matter © 2006 Elsevier B.V. All rights reserved.
doi:10.1016/j.jpowsour.2006.02.098

Nomenclature

D	diameter (m)
D_{eff}	diffusion effective coefficient ($m^2\ s^{-1}$)
E	nernst potential (V)
F	Faraday's constant ($C\ mol^{-1}$)
h_{cv}	convective heat transfer coefficient ($W\ m^{-2}\ K^{-1}$)
Δh_f	enthalpy of formation ($J\ mol^{-1}$)
i	current density ($A\ m^{-2}$)
i_0	exchange current density ($A\ m^{-2}$)
k_{cd}	conductive heat transfer coefficient ($W\ m^{-1}\ K^{-1}$)
K_{eq}	equilibrium constant
n	molar flow ($mol\ s^{-1}$)
n_e	number of exchanged electrons
Nu	Nusselt number
p	pressure (Pa)
Pr	Prandtl number
q	heat flow per unit area ($W\ m^{-2}$)
Q	total heat flow (W)
r	rate of reaction ($mol\ m^{-2}\ s^{-1}$)
R	gas constant ($J\ mol^{-1}\ K^{-1}$)
Re	Reynolds number
S	cell active area (m^2)
STCR	steam to carbon ratio
t	thickness (m)
T	temperature (K)
U_f	fuel utilization factor
x	axial coordinate (m)
$x_{t.e.}$	thermal entry length (m)
Δx	slice length (m)
$[X]$	concentration of X

Greek letters

α	transfer coefficient (activation loss)
α_{gas}	gas absortivity
γ	pre-exponential factor
ε	emissivity
ρ	resistivity ($\Omega\ m$)
σ	Steffan-Boltzmann's contant

Subscripts

a	anode
act	activation
c	cathode
cd	conduction
con	concentration
cv	convection
e	electrolyte
eq	equilibrium
f	formation
h	hydraulic
ohm	ohmic
ref	methane reforming reaction
shift	shift reaction
0	standard

Superscripts

0	bulk flow
*	active site

Table 1
Reference geometry

Length (m)	1.5
Anode outer diameter (mm)	22
Anode thickness (μm)	100
Electrolyte thickness (μm)	40
Cathode thickness (mm)	2.2
Metallic interconnection thickness (μm)	85
Active area (cm^2)	834

is far less than with conventional plants due to the increase in efficiency.

Fuel cells are thought as excellent complements to heavy duty power plants in the mid and long term but their technology must be improved in many ways so that both performance and reliability increase while cost remarkably decreases. Control of temperature inside high temperature fuel cells, as well as forecast of mechanical failures caused by temperature oscillations must be studied in detail. To do so, a model of performance is needed. This model must give a precise description of every electrochemical and heat transfer process taking place inside the cell.

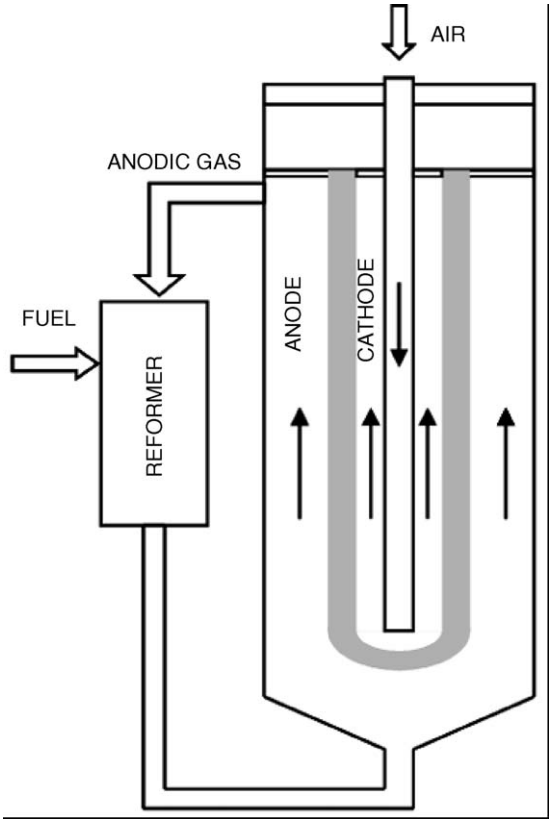

Fig. 1. Schematic view of power plant.

Finally, a fuel conditioning system is needed. Although internal reforming of natural gas is possible when dealing with high temperature fuel cells, part of the fuel flow must be reformed before it enters the anode of the fuel cell.

The work presented here covers all the subjects mentioned above and gives a very valuable tool to further develop the tubular solid oxide fuel cell technology. Although the model is fully flexible and applicable to tubular cells with any dimensions, a hundred watt Siemens-Westinghouse cell has been considered as base case; see Table 1 [1]. In addition, a prereformer fed with natural gas and anode exhaust gas is included. A schematic view of the plant can be found in Fig. 1.

2. Fuel conditioning

2.1. Production of hydrogen

Natural gas, consisting mainly of methane, is the most interesting source of hydrogen for stationary applications of SOFCs [2]. Methane conversion to hydrogen and by-products can be done through different techniques, steam reforming being the most suitable if fuel cells are involved. In this case, when a stream of methane mixes with another one with a high content of water steam, the following reaction may take place:

$$CH_4 + H_2O \rightarrow 3H_2 + CO \quad (1)$$

Eq. (1) describes the reforming process and, since it is endothermic ($\Delta h_f = 206\,\mathrm{kJ\,kmol^{-1}}$), is usually coupled to high temperatures or to heat addition. Carbon monoxide, which is a by-product of the reforming reaction, is further oxidized to carbon dioxide if water is still present (Eq. (2))

$$CO + H_2O \rightarrow H_2 + CO_2 \quad (2)$$

This second reaction (Eq. (2)), named water gas shift reaction, is slightly exothermic ($\Delta h_f = -41\,\mathrm{kJ\,kmol^{-1}}$) and favours the formation of hydrogen.

Eq. (1) and (2) take place inside the anodic duct of an SOFC due to the high operating temperature of the cell and the high concentration of water steam in the anodic gas, which can be as high as 50%. This steam is formed when hydrogen is oxidized according to the following exothermic ($\Delta h_f = -242\,\mathrm{kJ\,kmol^{-1}}$) reaction:

$$H_2 + O_2 \rightarrow H_2O \quad (3)$$

Nevertheless, not only Eqs. (1)–(3) are possible and some other undesirable reactions can be found. In particular, decompositions of methane or carbon monoxide may take place through the following reactions:

$$CH_4 \rightarrow C + 2H_2 \quad (4)$$

$$2CO \rightarrow C + CO_2 \quad (5)$$

which are endothermic ($\Delta h_f = 75\,\mathrm{kJ\,kmol^{-1}}$) and exothermic ($\Delta h_f = -172.6\,\mathrm{kJ\,kmol^{-1}}$), respectively. If any of these two reactions took place at the anode, deposition of carbon particles over the anode surface would block the catalyst and dramatically reduce its activity; in such a case, the electrochemical performance of the cell would drop down.

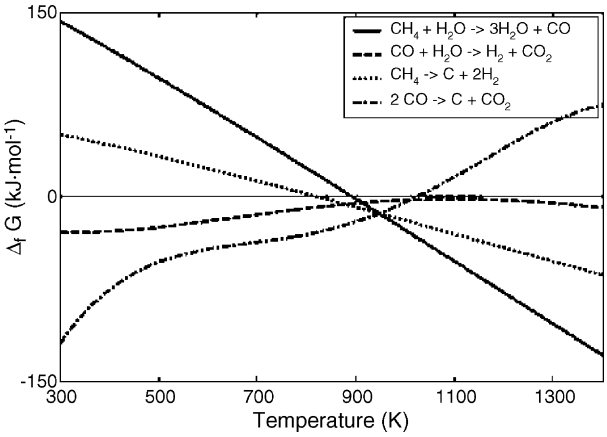

Fig. 2. Gibbs free energy change for reactions (1), (2), (4) and (5).

Temperatures around 950 °C enhance those reactions whose behaviour is more endothermic, i.e. Eq. (1), while decreasing the rate of exothermic reactions, specially Eq. (4) and, to a lesser extent, Eq. (2). Fig. 2 shows the variation of free energy for reactions Eqs. (1)–(2), (4)–(5) with temperature [3].

The changes in Gibbs free energy are related with the way in which a certain reaction occurs. In other words, a reaction whose Gibbs free energy change is positive at a certain temperature will shift towards reactants. Oppositely, the same reaction would shift towards products if the change in the Gibbs free energy of the system were negative at that temperature. The latter case is known as a spontaneous process. According to the relationship between Gibbs free energy and spontaneity, Fig. 2 shows that below 800 K, neither methane reforming nor decomposition are spontaneous processes; at this temperature, carbon monoxide is decomposed into particles and carbon dioxide rather than oxidized with water, Eqs. (5) and (2), respectively. Despite this, if temperature rises above 1100 K (850 °C), methane reforming and decomposition become spontaneous. Eq. (3) is spontaneous at any temperature.

Finally, the concentration of steam is increased in order to enhance the conversion of methane into hydrogen and not into atomic carbon. By doing this, and according to Le Chatelier's principle, the equilibrium of the reforming reaction is shifted to the products.

The exhaust gas of the anode is the most interesting source of both heat and steam for the reforming process inasmuch as its temperature is somewhere near 1000 °C and it contains up to 50% (v) of water steam. This gas is recirculated and mixed with the fuel before this enters the cell.

2.2. Prereforming

It has been stated that internal reforming of methane is possible in solid oxide fuel cells. However, if the anode is fed with pure methane temperature drops down significantly in the first part of the cell due to the endothermy of the reforming reaction. Later on, when methane is fully reformed to hydrogen, the heat

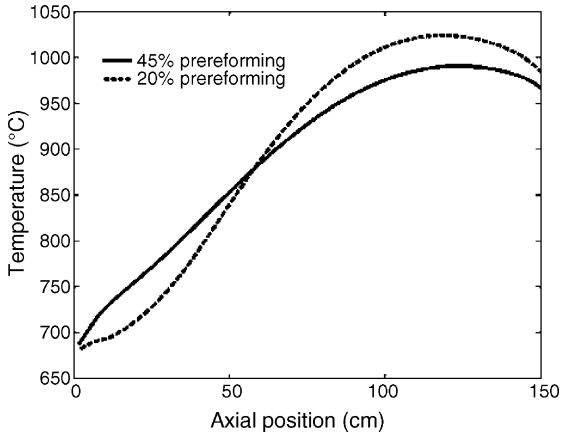

Fig. 3. Effect of prereforming on temperature of tube at 0.6 V and 80% fuel utilization.

released in Eq. (3) is no longer consumed by Eq. (1) and temperature increases; it must be taken into account that the total heat released by Eq. (3) doubles that consumed by Eq. (1) [4]. Besides, the initial temperature drop affects the electrochemical performance of the cell negatively and gives place to high thermal stresses, which can ruin the cell due to the combination of a significant temperature gradient along the tube and different thermal expansion coefficients of anode, cathode and electrolyte [5]. Consequently, methane must be partially reformed in an external reactor [2,4].

Fig. 3 shows that the evolution of tube temperature along the cell is smoother when the degree of prereforming is high. Nevertheless, this situation also leads to a drop in electrochemical performance so an intermediate working point must be adopted.

2.3. Prerefomer model

The prerefomer is a catalytic bed reactor fed by streams of natural gas and anodic exhaust gas. These gases react according to Eqs. (1) and (2) which are considered to reach equilibrium at the exit temperature. The composition of the effluent is defined by constants $K_{eq,ref}$ and $K_{eq,shift}$ which depend on temperature according to the polynomial in Eq. (8). Coefficients in Eq. (8) are different when applied to $K_{eq,ref}$ and $K_{eq,shift}$ and can be found in Table 2 [3,6,7]

$$K_{eq,ref} = \frac{[H_2]^3[CO]}{[CH_4][H_2O]} \quad (6)$$

Table 2
Coefficients in Eq. (8) [3,7]

	Reforming	Shift
a	-2.6312×10^{-11}	5.47×10^{-12}
b	1.2406×10^{-7}	-2.5748×10^{-8}
c	-2.2523×10^{-4}	4.6374×10^{-5}
d	1.9503×10^{-1}	-3.9150×10^{-2}
e	−66.1395	13.2097

$$K_{eq,shift} = \frac{[H_2][CO_2]}{[CO][H_2O]} \quad (7)$$

$$\log K_{eq} = aT^4 + bT^3 + cT^2 + dT + e \quad (8)$$

Recirculation of anode exhaust flow is done in order to avoid the problems mentioned before, the amount of anode exhaust flow to be recirculated being related to the molar flow of atomic carbon entering the reactor through the "steam to carbon ratio" or STCR. STCR is the ratio of steam molar flow to methane and carbon monoxide molar flow at the prereformer inlet

$$\text{STCR} = \left.\frac{n_{H_2O}}{n_{CH_4} + n_{CO}}\right|_{\text{inlet prereformer}} \quad (9)$$

According to Peters et al. [8], for STCR higher than 2/2.5 carbon deposition does not take place inside the prereformer.

The prereformer is considered to be adiabatic, i.e. no heat is transferred to or from the environment. Thus, the composition of the exhaust gas can be calculated by applying simultaneously the laws of conservation of mass and energy and the laws of chemical equilibrium (Eqs. (6)–(8)) at the exit of the reactor.

3. Fuel cell model

Fig. 1 shows reference geometry for the base case. Air enters the injector tube and flows downwards. At the end of the tube, the flow turns back to the upwards direction through the annular duct between the injector tube and the inner wall of the cathode. Parallel to it, a fuel stream coming from the prereformer flows upwards through the anode duct at the outer face of the cell tube. This layout can be thought of as coflow and is divided into a number of slices in the axial direction. Each one of these elements is divided again into five elements in the radial direction:

1. Air injector tube.
2. Air injector tube wall.
3. Annular duct (cathode).
4. Cathode–electrolyte–anode wall.
5. Anode duct.

The division made is standard for a finite volume method application to tubular cells and has been used, with few changes, by Campanari [1] and Stiller et al. [9] before. Fig. 4 shows a slice and its elements.

Axial symmetry is considered, both for the electrochemical and thermal models, on the basis of the distribution of tubes inside a fuel cell stack as shown in Fig. 5. A stack, in particular for a Siemens-Westinghouse cell, is formed by a number of bundles of 24 tubular cells on a 3×8 configuration. Those cells located in the core of the stack, A in Fig. 5, are surrounded by other cells working under similar conditions. In such cases, considering axial-symmetric boundary conditions is acceptable and the polar coordinate can be eliminated from the calculations. If the cell is located in the outer part of the stack, B in Fig. 5, axial-symmetric

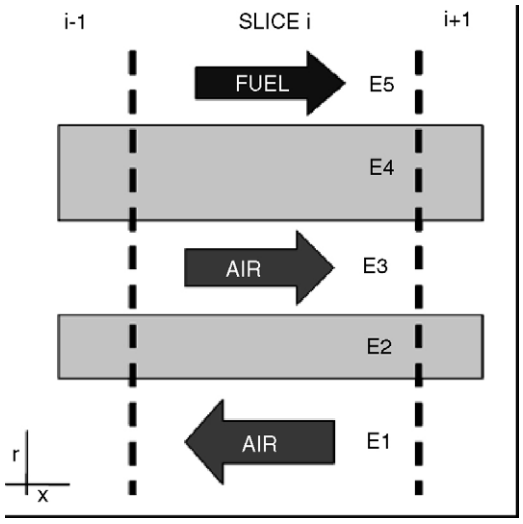

Fig. 4. Elements in a slice.

boundary conditions cannot be considered and a fully three-dimensional analysis must be done.

Fuel cell stacks are usually formed by a lot of tubes, say 1000 tubes per kilowatt, and most of them are located in its core so a hypothesis of axial symmetry is applicable to most of the tubes in a stack. However, if the effects of peripheral tubes are to be considered, some authors consider a 2–3% penalization in total power due to heat losses to the surroundings [10] according to Siemens-Westinghouse recommendations.

Finally, in order to decrease the computational load, the analysis of the cell is split into two blocks. Firstly, the cell electrochemical behaviour is studied and, for this purpose, a prescribed temperature condition is set so that the temperature field is invariable. Later, an analysis of heat transfer phenomena inside the fuel cell is done where current density, voltage loss, reaction rate distributions are known. Although both blocks can be solved independently, they are inseparables from a thermodynamic point of view. Fig. 6 shows that the solution to the analysis is single.

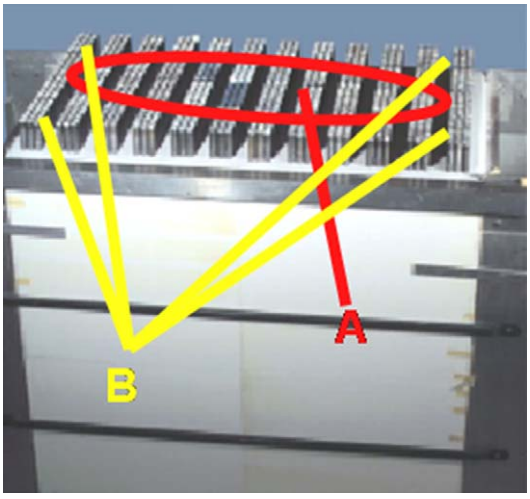

Fig. 5. Bundles in a fuel cell.

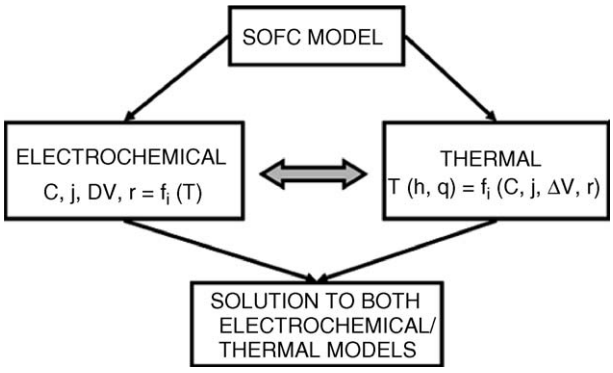

Fig. 6. Block solver.

4. Internal reforming

Previous to describing the fuel cell thermal and electrochemical models of performance some comments on methane internal reforming must be done. The anodic duct of a solid oxide fuel cell is fed by the effluent of the prereformer which consists mainly of hydrogen and water and has about 10–20% (v) of unreformed methane and carbon monoxide. As long as methane is still present two heats of reaction tend to heat up and cool down the circulating gas: heat released by the oxidation of hydrogen and consumed by the reforming of methane. Carbon deposition is again avoided due to the high temperature and content of steam.

The water gas shift reaction is considered to reach equilibrium, defined by constant $K_{eq,shift}$ (Eq. (7)), at each point of the duct. The temperature to be considered in Eq. (8) is that of the anodic gas at each point of the duct.

For the reforming reactions two scenarios are considered

1. Methane reforming reaches equilibrium. Under these circumstances, the analysis is similar to that of the prereformer. Eqs. (6)–(8) along with heat and mass balances are used to determine the equilibrium concentration at the anodic local temperature.
2. Methane reforming reaction is slow and equilibrium is not reached. The process is kinetically controlled. Ahmed and Fogger's [11] equation for the reforming rate is used in this case (Eq. (10))

$$r_{CH_4} = k_{ref} p_{CH_4}^{0,85} p_{H_2O}^{0,35} \exp\left(-\frac{95 \times 10^3}{RT}\right) \quad (10)$$

It must be pointed out that both hypotheses have been used before to describe the reforming process inside a high temperature fuel cell. Thus, Magistri et al. [12] assume equilibrium conditions while Campanari [1], Stiller et al. [9] or Selimovic [7] employ kinetic theory equations. However, the methodology presented in this work is a new approach to the internal reforming analysis as long as it takes into account that this process can be characterized by different mechanisms in different positions inside the cell.

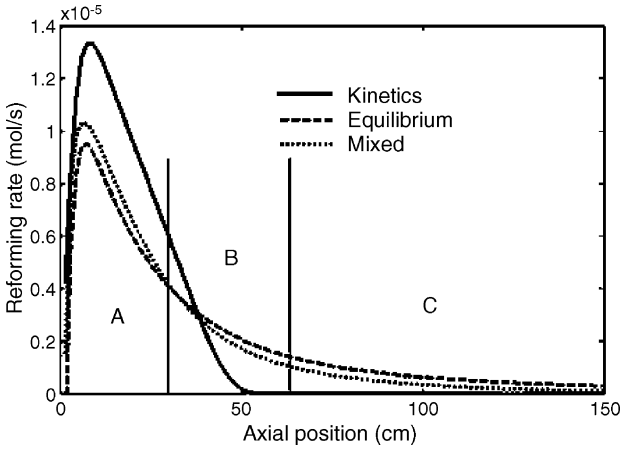

Fig. 7. Effect of reforming description on rate of reaction.

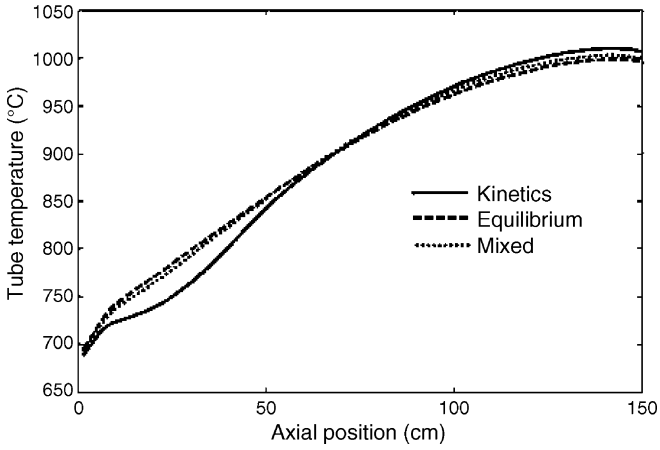

Fig. 8. Effect of reforming rate on tube temperature.

The following method is used to evaluate the reforming rate of reaction. First, the rate of reaction is calculated considering that equilibrium is reached. Then, this value is compared to that given by Eq. (10) after an iterative calculation to include the effect of water gas shifting. If the rate of reaction given by the kinetic theory is higher than that at equilibrium, equilibrium is reached. Else, equilibrium is not reached and Eq. (10) must be used. Fig. 7 shows the rates of reaction when each of the models proposed are used: equilibrium, kinetics and both. For the latter, the "mixed method" denomination has been used.

Tree different zones can be identified in Fig. 7. The first zone is marked A and ranges from 0 to 30 cm in the axial direction of the fuel flow. In this zone, the reforming process reaches equilibrium and the rate of reaction is determined by the equilibrium constant $K_{eq,ref}$. Oppositely, in zone C the process is controlled by kinetics because the rate of reaction is too slow due to a low concentration of methane and equilibrium is not reached; i.e. the rate of reaction assuming equilibrium is far higher than that predicted by Eq. (10). Zone B is a transition zone and temperature determines whether equilibrium is reached or not.

Fig. 7 shows that the rate of reaction when the "mixed method" is used is close, slightly above, to the rate predicted by an equilibrium hypothesis initially and close, again slightly above, to the rate of reaction calculated from Eq. (10) later on. The reason why the "mixed method" line does not coincide with the equilibrium and kinetics lines in zones A and C, respectively is that fuel and air flow in opposite directions so temperatures at one end of the tube strongly depend on temperatures at the other end. The influence of the reforming description on tube temperature is shown in Fig. 8.

Table 3 shows the effect of different descriptions of the reforming process on final results. Two conclusions can be drawn. The maximum error made when using any of the two usual descriptions, kinetics or equilibrium, is 1% on the main parameters of performance. Besides, Table 3 shows that assuming the reforming reaction at equilibrium underestimates power and efficiency while using Eq. (10) leads to an overestimation, in both cases with respect to the "mixed method", which is considered to be closer to reality as shown later.

Table 3
Effect of reforming description on results (pressure = 3 bar)

	Kinetics	Equilibrium	Mixed
Voltage (V)	0.6	0.6	0.6
Current density (A m^{-2})	3045	2988	3002
Fuel utilization (%)	81.2	79.7	80
Air utilization (%)	19.3	18.9	19
Power (W)	152.4	149.5	150.2
Efficiency (%)	46.44	45.56	45.79
Mean temperature (°C)	892	895	896
Peak temperature (°C)	1010	999	1003

5. Electrochemical model

According to the discretization shown above (Fig. 4), an electrochemical analysis based on deviations from ideal performance is proposed at each slice. Considering the electrodes to be equipotential surfaces [10,13], the ideal or Nernst voltage is defined by

$$E = E_0 + \frac{RT}{n_e F} \ln\left(\frac{p_{H_2} p_{O_2}^{1/2}}{p_{H_2O}}\right) \quad (11)$$

where E_0 is the standard potential, which varies almost lineally with temperature [3]

$$E_0 = 1.26485 - 2.4725 \times 10^{-4} T - 1.875 \times 10^{-8} T^2 \quad (12)$$

Irreversibilities, also known as polarizations or overpotentials, arise that cause voltage losses from the Nernst voltage value and have a negative impact on fuel cell performance. There are three types of overpotentials:

1. Activation loss: ΔV_{act}.
2. Ohmic loss: ΔV_{ohm}.
3. Concentration loss: ΔV_{con}.

Multidimensional models previously developed frequently include activation and ohmic losses but not concentration loss as this is one order of magnitude smaller under usual operating conditions.

5.1. Activation overpotential

Activation losses take place at the electrodes and are related to the minimum voltage drop needed to overcome the activation energy of both hydrogen and oxygen ion forming reactions. The activation overpotential for each electrode is usually defined by the Butler–Volmer equation

$$i = i_0 \left\{ \exp\left(\alpha_a \frac{n_e F \Delta V_{act}}{RT}\right) - \exp\left(\alpha_c \frac{n_e F \Delta V_{act}}{RT}\right) \right\} \quad (13)$$

where i_0, α_a and α_c are the exchange current density and transfer coefficients, respectively.

Charge transfer coefficients are related to the relative response of current density at each electrode to a change in activation overpotential. Evaluating these coefficients is a difficult task and they are usually considered symmetric and equal to 0.5 for a one-electron charge-transfer reaction [14]. In such a case, Eq. (13) can be rewritten as

$$i = 2i_0 \sinh\left(\frac{n_e F \Delta V_{act}}{RT}\right) \quad (14)$$

Eq. (14) can be further simplified assuming that activation losses are high, Tafel equation (Eq. (15)), or low, linear equation (Eq. (16))

$$\Delta V_{act} = a + b \ln i \quad (15)$$

$$\Delta V_{act} = \frac{RT}{n_e F i_0} i \quad (16)$$

Activation losses are considered low if Eq. (17) is satisfied [7]

$$\frac{F \Delta V_{act}}{n_e RT} < 1 \quad (17)$$

However, this symmetric relationship of charge transfer coefficients is not based on any physical law and the only accurate way of determining α_a and α_c is to do some testing. In fact, it is not even clear whether transfer coefficients are constant for a given fuel cell and reaction or they depend on current density. For these reasons, data from tests done by Costamagna and Honegger [15] on SOFCs have been used and simplifications of Butler–Volmer equation have been discarded in this work. It must be said that calculating activation overpotentials from simplified equations can lead to errors as high as 23% as shown by Chan et al. [16].

The exchange current density is related to the current density exchanged back and forth when equilibrium is reached and is not easy to evaluate either [14]. Despite this, there is agreement that the following reactions are appropriate for anode (Eq. (18)) and cathode (Eq. (19)):

$$i_{0,a} = \gamma_a \left(\frac{p_{H_2}}{p_{ref}}\right)^a \left(\frac{p_{H_2}}{p_{ref}}\right)^b \exp\left(-\frac{E_{act,a}}{RT}\right) \quad (18)$$

$$i_{0,c} = \gamma_c \left(\frac{p_{O_2}}{p_{ref}}\right)^c \exp\left(-\frac{E_{act,c}}{RT}\right) \quad (19)$$

Pre-exponential factors, exponents a, b and c and activation energies are taken from tests by Costamagna and Honegger [15]. The complexity of evaluating charge transfer coefficients is applicable to the coefficients involved in Eqs. (18) and (19).

5.2. Ohmic overpotential

Ohmic overpotential is caused by the flow of electric charge across electrodes and electrolyte. It can be defined by

$$\Delta V_{ohm} = i R_{ef} \quad (20)$$

where R_{ef} is taken as an effective electric resistance similar to that of the structure formed by electrolyte, electrodes and interconnection plates. Complexity of current flow paths inside the cell makes it difficult to evaluate an equivalent resistance. In this work, the model developed by Nisancioglu [17], and previously used by Haynes [10], Campanari [1] and Stiller et al. [9], has been completed with a temperature dependence of electronic/ionic resistivities which was not included in [17]. This dependence is taken from ref. [7] and can be expressed by the following equation:

$$\rho_i(T) = \frac{T}{A} \exp\left(\frac{B}{T}\right) \quad (21)$$

where A and B depend on materials.

5.3. Concentration losses

Concentration overpotential is related to the velocity at which diffusion of species takes place inside porous electrodes. Generally speaking, it can be said that there are two main targets for electrode designers. First, it is important that electrodes be thin because the thinner the layer through which species diffuse, the faster the hydrogen oxidation reaction and the higher the current density of the cell. The lower limit of electrode thickness is determined by available manufacturing techniques and mechanical integrity matters. Besides, operating conditions have a notorious impact over concentration polarization. In particular, species flows at each electrode are caused by concentration gradients between bulk flow and active sites. For this reason, when one of the reactants is near to exhaustion, the whole cell performance is controlled by the slower diffusion process what causes a higher voltage drop. This situation can also be found if any of the reactants is near to 100% conversion or if current density becomes too high.According to Selimovic [7], concentration overpotential can be evaluated from the following expression:

$$\Delta V_{con} = \frac{RT}{n_e F} \ln\left(\frac{p^*_{H_2} p^0_{H_2O}}{p^0_{H_2} p^*_{H_2O}}\right) + \frac{RT}{n_e F} \ln\left(\frac{p^*_{O_2}}{p^0_{O_2}}\right) \quad (22)$$

where superscripts "0" and "*" stands for properties at free bulk flow and active sites, respectively. If concentration losses are to be known, properties at active sites must be related somehow to free flow properties as long as only these are known when analysing the cell. Fick's laws are used to evaluate concentrations at active sites from free flow concentrations. For this purpose, effective diffusion coefficients are developed.

The calculation of diffusion coefficients is out of the scope of this paper and would not be described. Still, it must be said that

calculating diffusion coefficients of gases which are part of either cathodic or anodic flows is a difficult task. Experimental data are very scarce and, where available, they are taken at very low temperatures compared to that inside an SOFC. This situation gets worse when applied to binary diffusion coefficients.

A solution to this problem has usually been found in using semi-empirical, theoretically based methods, which extend available data to practical operating conditions. Lennard Jones' method for binary coefficients is the most popular and extended, although Todd and Young [18] show that using this method leads to remarkable deviations from experimental data at high temperature. Instead, Fuller et al.'s method is shown to be much more accurate, especially at high temperature, what makes it suitable for fuel cell modelling.

Eq. (23) and (24) are obtained when applying Fick's laws as described in [19] and represent concentration losses at cathode and anode, respectively

$$\Delta V_{\mathrm{con,c}} = \frac{RT}{n_{\mathrm{e}}F}\ln\left(\frac{1}{x^0_{\mathrm{O_2}}} - \left(\frac{1}{x^0_{\mathrm{O_2}}} - 1\right)\exp\left(\frac{iRTt_{\mathrm{c}}}{2n_{\mathrm{e}}FD_{\mathrm{ef,c}}p}\right)\right) \tag{23}$$

$$\Delta V_{\mathrm{con,a}} = \frac{RT}{n_{\mathrm{e}}F}\ln\left(\frac{1 - \frac{iRt_{\mathrm{a}}}{2FD_{\mathrm{ef,a}}x^0_{\mathrm{H_2}}p}}{1 + \frac{iRt_{\mathrm{a}}}{2FD_{\mathrm{ef,a}}x^0_{\mathrm{H_2O}}p}}\right) \tag{24}$$

5.4. Mass balance

Once ideal voltage and polarizations are known, operating voltage throughout the cell can be evaluated from Eq. (25)

$$V = E - \Delta V_{\mathrm{act}} - \Delta V_{\mathrm{ohm}} - \Delta V_{\mathrm{con}} \tag{25}$$

Given the operating voltage and temperature field of the cell, the latter being part of the solution to the thermal model, there is only one value of current density satisfying Eq. (25) at each slice. It must be said that although some models use average current density along the cell to establish operating conditions in order to diminish computational time, this do not correspond to real operation of a fuel cell. Instead, a single voltage is set at desired value and current density adjusts to satisfy Eq. (25) according to existing temperatures and concentrations inside the cell. The model presented here is based on real operating conditions so voltage will be an input for any simulation.

A continuity equation must be applied at each slice after solving Eq. (25). To do so, variations of species molar flow due to methane reforming, water gas shift and/or hydrogen oxidation must be calculated. Both reforming and shift are evaluated according to Sections 2 and 4 with values shown in Table 4. Conversion rate of hydrogen, oxygen and water due to electrochemical oxidation is calculated thanks to Faraday's law

$$\Delta\dot{n}_{\mathrm{H_2}} = -\frac{iS}{n_{\mathrm{e}}F} = -\Delta\dot{n}_{\mathrm{H_2O}} = 2\Delta\dot{n}_{\mathrm{O_2}} \tag{26}$$

Finally, the expression of the principle of conservation of mass to be applied at each slice and for each component of each stream is

$$\dot{n}_{\mathrm{outlet}} = \dot{n}_{\mathrm{inlet}} + \Delta\dot{n}_{\mathrm{oxid}} + \Delta\dot{n}_{\mathrm{ref}} + \Delta\dot{n}_{\mathrm{shift}} \tag{27}$$

The mass balance is coupled to an energy balance at the same control volume, which comes from the application of a thermal model to heat transfer phenomena inside the cell.

Table 4
Input parameters to model

Anode resistivity (Ω m) (Eq. (21))	$\rho_{\mathrm{a}} = (T/95 \times 10^6)\exp(-1150/T)$
Cathode resistivity (Ω m) (Eq. (21))	$\rho_{\mathrm{c}} = (T/42 \times 10^6)\exp(-1200/T)$
Electrolyte resistivity (Ω m) (Eq. (21))	$\rho_{\mathrm{e}} = (1/3.34 \times 10^4)\exp(-10300/T)$
Interconnection resistivity (Ω m) (Eq. (21))	$\rho_{\mathrm{icm}} = (T/9.3 \times 10^6)\exp(-1100/T)$
Anode conductivity ($\mathrm{W\,m^{-1}\,K^{-1}}$)	3
Cathode conductivity ($\mathrm{W\,m^{-1}\,K^{-1}}$)	3
Electrolyte conductivity ($\mathrm{W\,m^{-1}\,K^{-1}}$)	3
Anode emissivity	0.9
Cathode emissivity	0.9
Butler–Volmer, anode (Eq. (13))	$\alpha_{\mathrm{a}} = 2$, $\alpha_{\mathrm{c}} = 1$
Butler–Volmer, cathode (Eq. (13))	$\alpha_{\mathrm{a}} = 1.4$, $\alpha_{\mathrm{c}} = 0.6$
Exchange current density, anode (Eq. (18))	$\gamma_{\mathrm{a}} = 5.5 \times 10^{10}$ ($\mathrm{A\,m^{-2}}$), $a = 1$, $b = 1$, $E_{\mathrm{act,a}} = 120\,\mathrm{kJ\,kmol^{-1}}$
Exchange current density, cathode (Eq. (19))	$\gamma_{\mathrm{c}} = 7 \times 10^9$ ($\mathrm{A\,m^{-2}}$), $c = 1$, $E_{\mathrm{act,c}} = 120\,\mathrm{kJ\,kmol^{-1}}$
Methane reforming (Eq. (10))	$k_{\mathrm{ref}} = 8542\,\mathrm{mol\,bar^{-0.5}\,s^{-1}\,m^{-2}}$

6. Thermal model

High heat flows are found inside an SOFC due to highly exothermic and endothermic reactions taking place. In particular, the heat released in the oxidation of hydrogen is mainly used to (i) heat the air flowing through the air supply pipe and (ii) enhance methane reforming at the anode.

Heat flows must be controlled due to mechanical integrity issues as the solid structure of the cell is formed by three very thin layers whose thicknesses range from 40 μm to 2 mm and with thermal expansion coefficients between 10 and $13 \times 10^{-6}\,^{\circ}\mathrm{C}^{-1}$. If the temperature gradient along the solid tube is too steep, thermal expansion mismatches will lead to poor performance and, eventually, to mechanical failure. For these reasons, it is necessary to have a highly detailed multidimensional thermal model in order to simultaneously search for high efficiency and reliability.

The following heat transfer mechanisms has been considered and applied to control volumes in Fig. 4:

1. Axial heat conduction inside the solid structure of both cell and air supply pipe.
2. Radial heat convection at free surfaces including inner and outer walls of cell and air supply pipe.
3. Radial heat radiation between cathode inner and air supply pipe outer walls.
4. Radial heat radiation between anodic gas and anode outer wall.

6.1. Conduction

Solid structures are considered to be isothermal in the radial direction due to their negligible thickness. Axially, Fourier's law

is used to determine the heat flow per unit area perpendicular to the flow

$$q_{\text{cond}} = -k_{\text{cd}} \frac{\partial T}{\partial x} = -k_{\text{cd}} \frac{\Delta T}{\Delta x} \tag{28}$$

Estimating thermal conductivity k for a multilayer structure is a difficult task. However, a first guess can be done by considering the average conductivity as proportional to the conductivity and thickness of each layer (Eq. (29))

$$\bar{k}_{\text{cd}} = \frac{k_{\text{cd,c}} t_{\text{c}} + k_{\text{cd,e}} t_{\text{e}} + k_{\text{cd,a}} t_{\text{a}}}{t_{\text{a}} + t_{\text{e}} + t_{\text{c}}} \tag{29}$$

This approach is not rigorous because the average thermal conductivity should be closer to that of the layer acting as thermal barrier or insulator. However, an analysis of ceramic materials typically used in electrodes and electrolyte manufacturing reveals that thermal conductivity ranges from 2 to 4 $\text{W K}^{-1}\,\text{m}^{-1}$, with an average value of 3 for each layer [3]. Thus, the error made when using Eq. (29) to evaluate the average solid structure conductivity is negligible, even if conductivity is different from one layer to another (but into the range mentioned before). Finally, thermal conductivity of air supply pipe is considered to be a function of temperature [1].

6.2. Convection

An accurate study of convective heat transfer is absolutely necessary if maximum temperature of electrodes and electrolyte are not to be exceeded. It must be noted that mean operating temperature and maximum temperature are very close, say 900 and 1100 °C, respectively. Besides, convective heat transfer phenomena at thermal entries may be the cause of steep temperature gradients and, consequently, thermal stresses.Newton's law of cooling has been used to evaluate the heat flow per unit area

$$q_{\text{cond}} = h_{\text{cv}}(T_{\text{sup}} - T_{\text{gas}}) \tag{30}$$

where h_{cv} is the convective heat transfer or film coefficient.

The procedure to obtain the film coefficient at each one of the surfaces is quite similar. Firstly, physical properties of gases in contact with each surface are calculated: specific heat, viscosity and thermal conductivity. According to the work by Todd and Young [18] the specific heat of a mixture of gases is proportional to the specific heat and concentration of its species. The specific heat of each component of the mixture depends on temperature as a fifth order polynomial while the dependence of viscosity and thermal conductivity on temperature and composition is more complex. In particular, Reichenberg's and Wassiljeva's expressions are used to evaluate composition and thermal conductivity, respectively, although the scarce data for conductivity at high temperature may lead to not negligible errors.

In second place, Reynolds number is determined locally, for each stream and each slice. For this purpose, it is very important that the geometry of each duct be properly defined, specially the anodic duct whose complex geometry is shown in Fig. 9. In this case, the hydraulic diameter is calculated from the general

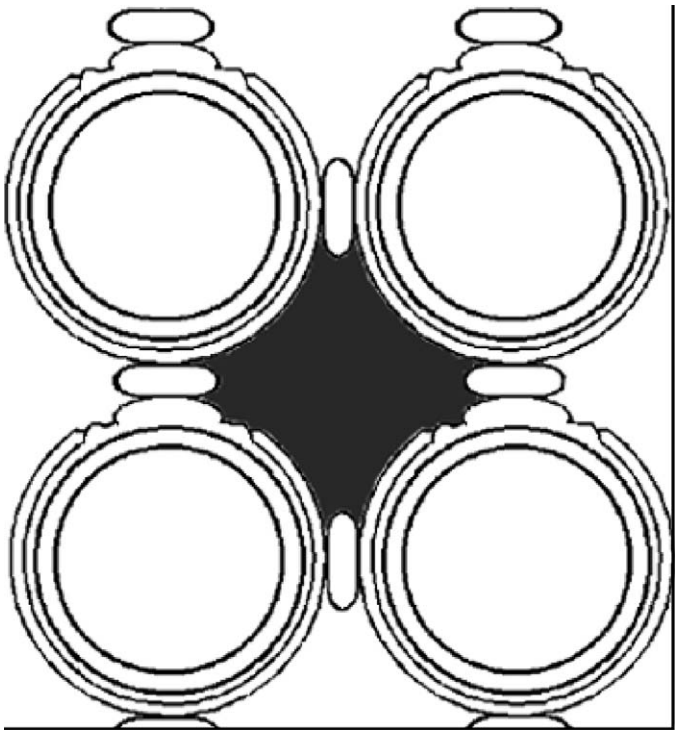

Fig. 9. Cross-sectional view of anodic duct.

expression

$$D_{\text{h}} = 4 \frac{\text{cross section}}{\text{wet perimeter}} \tag{31}$$

Next step after calculating Reynolds number is determining the regime of heat transfer inside the duct. Three cases are considered:

1. Laminar heat transfer, thermal and hydrodynamic entry length.
2. Laminar heat transfer, fully developed flow.
3. Turbulent heat transfer, fully developed flow.

Thermal and hydrodynamic boundary layers are considered to develop at the same time as long as Prandtl number is near to unity, above 0.7. The critical Reynolds number, based on duct hydraulic diameter, is taken as 2300 [20] and the thermal entry length for laminar flow is given by the following equation [20,21]:

$$x_{\text{t.e.}} = 0.0575 Re Pr D_{\text{h}} \tag{32}$$

Where the flow is turbulent, the thermal entry length is taken as negligible according to [21].

Average Nusselt numbers are usually evaluated from Re, Pr and duct geometry through empirical expressions. Nevertheless, this approach is not used in the present model as it is not accurate for a local heat transfer analysis. Instead, correlations for local Nusselt number Nu are used. Values of Nu in the thermal entry region are given by Rohsenhow et al. [20] while a constant value of 3.657 is assumed for fully developed laminar flow. Finally, Gnielinski equation for Nu is used where flow is

turbulent because of its great advantages [21]. Usually, correlations for forced convection, internal flow are not applicable to transition flows, i.e. *Re* ranging from critical value to about 10,000, due to uncertainty about flow behaviour but, in spite of this and according to Baehr and Stephan [21], Gnielinski equation is valid for *Re* above 2300. Besides, this correlation is more accurate with respect to experimental data than others, which are much simpler, like Dittus Boelter's.

The convective heat transfer coefficient can be easily evaluated from *Nu*

$$h_{cv} = \frac{k_{cd,gas} Nu}{D_h} \tag{33}$$

6.3. Radiation

The analysis of radiative heat transfer is compulsory if an accurate fuel cell model is to be developed, the main reasons for such a statement being a high view factor between injector tube and cathode and the high temperatures of these elements. Radiation inside the cell has two different locations: annular duct between cathode and air injector tube and anodic duct.

6.3.1. Radiation exchange between grey walls

In the annular duct radiative exchange between grey surfaces takes place, from the inner face of the cathode to the outer side of the injector tube. This phenomenon inside fuel cells has already been included in some of the models developed by other authors before [9,13,22–24] and no innovations are introduced here. Grey walls satisfying Kirchhoff's laws are considered. View factors are easily evaluated and emissivity is taken as 0.9 for both surfaces. The total heat flow exchanged by radiation between cathode and air supply pipe at each slice is

$$Q_{rad} = \frac{\sigma(T_{cathode}^4 - T_{injector}^4)}{\frac{1}{\varepsilon_{cathode}} + \frac{D_{cathode}}{D_{injector}}\left(\frac{1}{\varepsilon_{injector}} - 1\right)} \pi D_{cathode} \Delta x \tag{34}$$

Radiative exchange between walls is not considered in the anodic duct (Fig. 9) because, due to symmetric boundary conditions, all walls are considered to be at the same temperature. Radiation heat transfer does exist but the net heat flux at each wall is zero.

6.3.2. Grey gas radiation

Radiative heat transfer between a gas volume and a wall is usually negligible except if the optical thickness of the volume is very high or if some particular gases like carbon dioxide and/or water steam are present. For the scope of this work, the latter condition is satisfied in the anode as the fuel gas has up to 75% (v) of water and carbon dioxide. The molar fraction of these species in the cathodic gas is negligible and this consideration does not apply to radiation in the annular/cathodic duct.

Radiation between gases and walls has already been studied by some authors before [25,26] but these works present some lack of accuracy in the theoretical treatment of the gas properties. VanderSteen and Pharoah [25] used a CFD tool to analyze the influence of both kinds of radiation on the simulation. Results showed that radiation between walls must always be considered. With respect to participating media, they concluded that their influence might not be negligible under certain operating conditions. Samuelsen [26] included the effect of grey gases in all ducts.

Table 5
Coefficients for Hadvig's equation [27]

I	k_i	$b_{1,i} \times 10^1$	$b_{2,i} \times 10^4$	$b_{3,i} \times 10^7$	$b_{4,i} \times 10^{11}$
CO_2					
1	0.3966	0.4334	2.620	−1.560	2.565
2	15.64	−0.4814	2.822	−1.794	3.274
3	394.3	0.5492	0.1087	−0.3500	0.9123
H_2O					
1	0.4098	5.977	−5.119	3.042	−5.564
2	6.325	0.5677	3.333	−1.967	2.718
3	120.5	1.800	−2.334	1.008	−1.454

$C = f(T) = b_1 + b_2 T + b_3 T^2 + b_4 T^3$ (T in K)

Both of these works use simplified methods for estimating properties of gases but none of them with sufficient accuracy. VanderSteen and Pharoah studied four cases ranging from no heat absorption from gases to gases with high absorption coefficients but did not study the properties of gases as functions of composition, temperature and geometry. Samuelsen considered the dependence of properties on composition and temperature using the work by Hottel and Sarofim [20,21] and assumed that gases satisfy Kirchhoff's laws in order to simplify equations.

In this work, properties of gases are determined more rigorously. Emissivity and absorptivity of the anodic gas depend on its composition, temperature and on the geometry of the duct through the mean beam length, being Hottel's graphical method the easiest way to calculate them. Nevertheless, Hottel's method is not accurate enough and Hadvig's analytical method for calculating the emissivity of a gas mixture [27] is used

$$\varepsilon_{gas} = \varepsilon_{CO_2} + \varepsilon_{H_2O} - \varepsilon_{CO_2}\varepsilon_{H_2O} \tag{35}$$

The emissivity of each gas is evaluated from the following equation:

$$\varepsilon_i = \sum_{i=1}^{3} C_i (1 - \exp(-k_i p_i L)) \tag{36}$$

where p_i is the gas partial pressure and L the mean beam length. Coefficients for Eq. (36) can be found in Table 5.

The following equation given in [28] is used to evaluate the absorptivity of the gas considering that gases do not obey Kirchhoff's laws

$$\alpha_{gas} = \varepsilon_{CO_2}\left(\frac{T_{gas}}{T_{surface}}\right)^{0.65} + \varepsilon_{H_2O}\left(\frac{T_{gas}}{T_{surface}}\right)^{0.45} - \varepsilon_{CO_2}\varepsilon_{H_2O} \tag{37}$$

Using these radiative properties of the anodic gas, the heat flow exchanged between gas and surface per unit area can be calculated

$$q_{rad} = \frac{\varepsilon_{surface}\sigma}{1 - (1 - \alpha_{gas})(1 - \varepsilon_{surface})}(\varepsilon_{gas} T_{gas}^4 - \alpha_{gas} T_{surface}^4) \tag{38}$$

where all the walls of the anodic duct are supposed to be at the same temperature, as said before.

6.4. Energy balance

Solving energy balance equations at each volume of each slice gives the temperature distribution inside the cell. The following phenomena must be taken into account:

1. Molar mass variations due to gas flow inside ducts.
2. Heat release and/or consumption due to reforming, shift and/or oxidation reactions.
3. Heat transfer through conduction, convection and radiation.
4. Heating due to Joule effect at electric current conductors, i.e. cathode, anode and electrolyte.

The solution to the electrochemical model is used as an input to the thermal model in order to obtain distributions of temperature, heat flow and heat transfer coefficients as shown in Fig. 6. More information can be found in [19].

7. Validation

The validation of the model is a two step process. First, a validation of the global performance of the cell is done by comparing *V–I* curves from tests with those obtained by the model. This comparison (Fig. 10) shows good agreement between data published by Siemens-Westinghouse from tests on atmospheric cells [29] and results of the model presented. The model is therefore capable of predicting the performance of the tubular fuel cell with accuracy.

Besides the validation made in Fig. 10, a numerical evaluation of the model has been done. In particular, results from the model at atmospheric and overpressure operation have been compared with those in reference [1] which correspond to available data from tests published elsewhere. This comparison is shown in Table 6 along with the error made for each parameter.

According to errors shown (Table 6), which are smaller than 5% for the most important data, the model developed is accurate. In addition, it is remarkable that errors decrease considerably when pressure rises because this means that the model can be applied to fuel cell-gas turbine hybrid systems with minimal deviations from real performance. This fact, along with curve fitting in Fig. 10, suggests that the accuracy of the model presented above is satisfactory.

Table 6
Validation (p = 1.05/3.5 bar)

	Test	Simulation	Error (%)
Voltage (V)	0.69/0.64	0.69/0.64	–
Current density (A m^{-2})	1800/3000	1905/2926	5.8/2.5
Power (W)	104.8/157	109.6/157	4.6/0.5
Fuel utilization (%)	69/69	71.3/68.2	3.3/1.1
Air utilization (%)	17.8/23.8	18.6/23.4	4.5/1.7

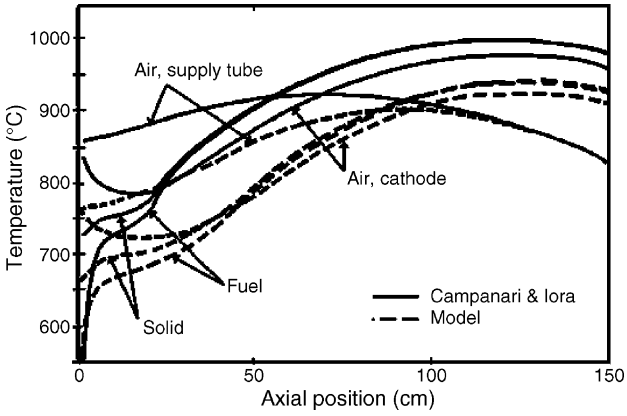

Fig. 11. Comparison of temperature distribution, data from ref. [1].

A direct experimental validation of the thermal model is not possible as long as there are no data available for the temperature field inside the cell. Only tests conducted by Hirano et al. [30] show temperature measurements at three relevant points of a tubular cell: initial, middle and end points. However, results are not comparable since the cell tested by Hirano et al. is a 30 cm long cell fed mainly with hydrogen, just 1% methane. Instead, a comparison with a previous model by Campanari and Iora [1] is presented in order to evaluate the accuracy of the model developed. The reference model is similar to that presented here with two main differences: the reforming process is assumed to be kinetically controlled and gas radiation is not considered. Figs. 11 and 12 show temperature and anodic gas composition distributions obtained by both models; similarity is observed but

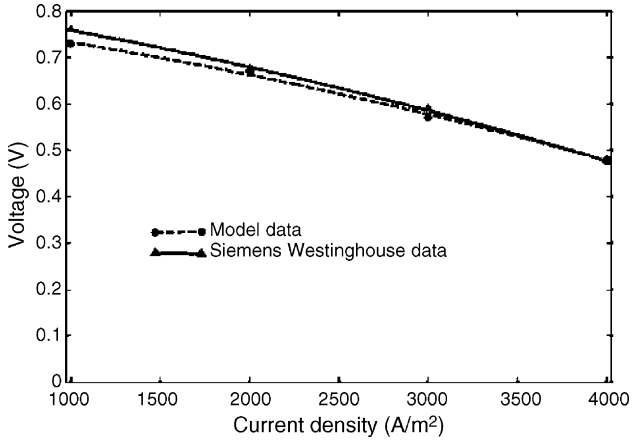

Fig. 10. Comparison with data from Siemens-Westinghouse [29].

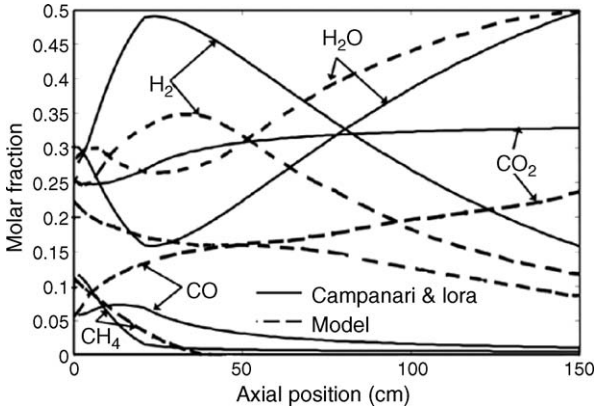

Fig. 12. Comparison of anode gas composition, data from ref. [1].

Table 7
Effect of anodic gas radiation

	Gas radiation	No gas radiation
Voltage (V)	0.6	0.6
Current density (A m^{-2})	3002	3003
Fuel utilization (%)	80	80
Air utilization (%)	19	19
Power (W)	150.2	150.2
Efficiency (%)	45.8	45.8
Mean temperature (°C)	896	897
Peak temperature (°C)	1003	1003

Case 1: 0.6 V, $U_f = 80\%$, $p = 3$ bar.

Table 8
Effect of anodic gas radiation

	Gas radiation	No gas radiation
Voltage (V)	0.2	0.2
Current density (A m^{-2})	8031	8097
Fuel utilization (%)	60.2	60.7
Air utilization (%)	8.8	8.9
Power (W)	134	135.1
Efficiency (%)	11.5	11.6
Mean temperature (°C)	599	903
Peak temperature (°C)	1014	1018

Case 2: 0.2 V, $U_f = 60\%$, $p = 3$ bar.

not coincidence. The differences are thought to be caused by the improvements made as they are located in the first part of the cell where reforming is at equilibrium (Figs. 7 and 8).

8. Effect of anodic gas radiation

Two main subjects have been introduced in this model with respect to previous works: a mixed method to evaluate the rate of reforming and the anodic gas radiation. The former has been studied in Section 4 and its influence has been evaluated both quantitatively and qualitatively. The effect of including radiation between anodic gas and anode outer surface is now analyzed.

Two cases are considered, high fuel utilization and low current density and vice versa; pressure is set at 3 bar for both cases. First, operation at 0.6 V and 80% fuel utilization is analyzed for anodic gas taking part in the radiative heat transfer and not. The results of both simulations are shown in Table 7 and it is concluded that for low current density the effect of grey gas radiation is negligible.

Table 8 shows results for the second case, 0.2 V and 60% fuel utilization. Now, results do not coincide when gas radiation is considered or not as including the effect of gas radiation leads to poorer performance by around 1%. The reason for this behaviour is the increased fuel mass flow. When current density is high, fuel mass flow increases, the anodic gas has more heat absorption capacity and its effect as heat sink is higher, resulting in a drop in cell temperature. This decrease in temperature affects to the electrochemical performance of the cell negatively as long as overpotential increase, mainly ohmic and activation overpotentials.

The conclusion to the comparison shown is that anodic gas radiation has a negligible effect on performance under normal operating conditions. Fuel cells are usually operated at high voltage and low current density seeking for high efficiency although it may be interesting to increase current density if high power density is sought, despite the loss in efficiency. However, if fuel flow increases, the effect of gas radiation may not be negligible and should be considered. This situation is usually related to high pressure, low voltage and low fuel utilization (Table 8).

9. Sensitivity analysis to fuel utilization factor

The model developed allows for a full sensitivity analysis of all the parameters determining the operating conditions of the cell. In particular, the effect of fuel utilization shown below is part of a complete analysis that can be found in [19]. The fuel utilization factor of a fuel cell accounts for the fraction of fuel which feeds the anode and is used to produce electrical work (Eq. (39)). It must not be taken as a sort of efficiency

$$U_f = \frac{\dot{n}_{H_2}|_{used}}{\dot{n}_{H_2,equivalent}|_{inlet}} \tag{39}$$

The influence of fuel utilization on cell performance is significant as depicted in Fig. 13, which shows the voltage–current density curve for two values of this parameter. It is important to note that the effect of increasing fuel utilization is not the same at high or low current densities.

An analysis of fuel cell internal performance has been done in order to understand Fig. 13. The Nernst potential depends on temperature and composition as shown above (Eqs. (11) and (12)). Figs. 14–16 depict the distribution of these parameters along the cell, temperature being drawn only for the solid structure.

Nernst potential increases with hydrogen and oxygen concentrations and decreases with water concentration (Eq. (11)). Thus, according to Figs. 14 and 15, the potential at 90% fuel utilization should be higher for the first 50 cm of the cell despite the effect of oxygen concentration as this is diminished by a power to 0.5. For the second half of the cell, the potential should be

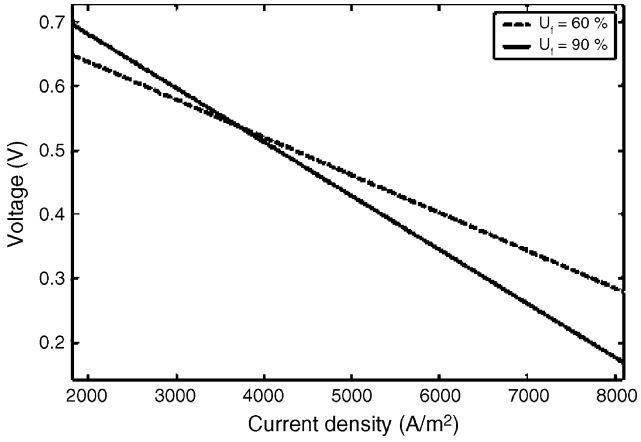

Fig. 13. Effect of fuel utilization on voltage–current density curve.

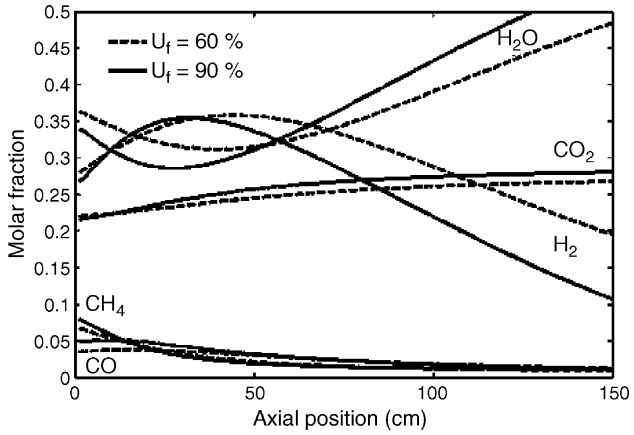

Fig. 14. Influence of fuel utilization on anodic gas composition, $V = 0.6$ V.

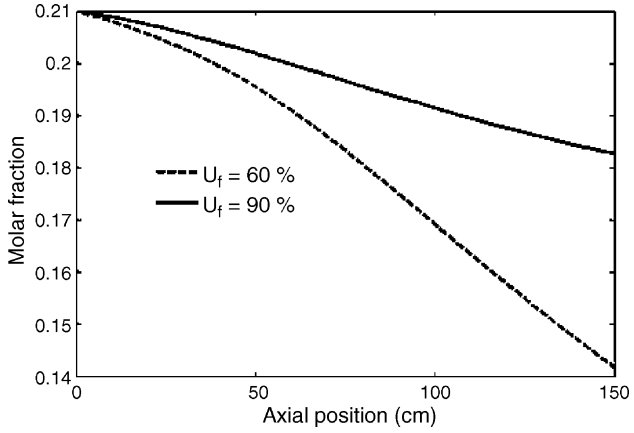

Fig. 15. Influence of fuel utilization on oxygen concentration at cathode, $V = 0.6$ V.

higher for 60% fuel utilization as concluded from compositions (Figs. 14 and 15).

The effect of fuel utilization on temperature is depicted in Fig. 16 where it can be seen that decreasing this parameter causes initial subcooling and final overheating with respect to normal values around 80%. When the fuel utilization factor is low, keeping voltage constant, there is a high fraction of fuel, which is not used for producing power. This fraction of fuel is not oxidized

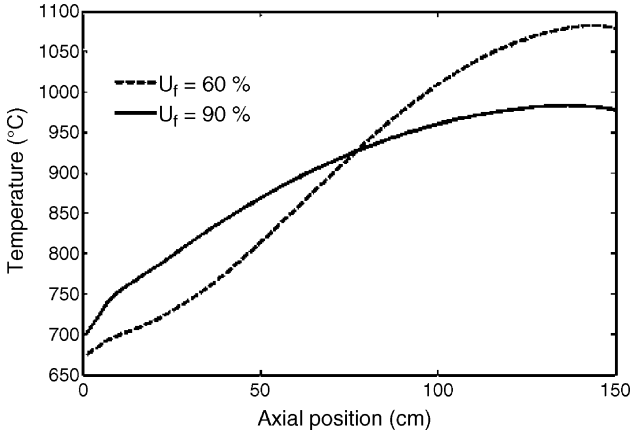

Fig. 16. Influence of fuel utilization on temperature of solid structure, $V = 0.6$ V.

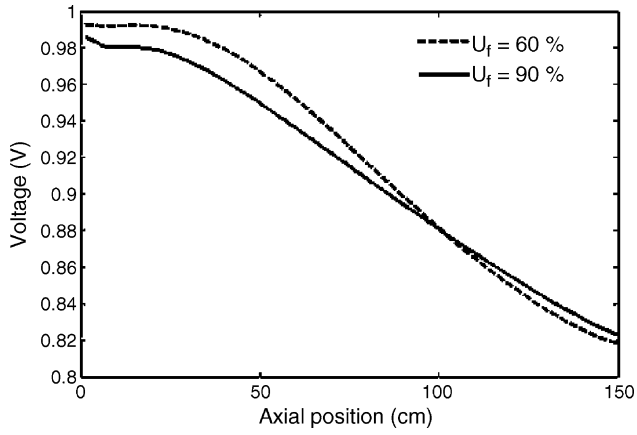

Fig. 17. Influence of fuel utilization on Nernst potential, $V = 0.6$ V.

but it is reformed, originating a significant decrease in temperature in the first part of the cell. The increase in temperature in the second half of the cell is caused by a lack of cooling air, considering that the average operating temperature and boundary conditions for natural gas and air streams feeding the cell are the same for all cases. The Nernst potential is directly affected by these changes in temperature (Eq. (12)), decreasing where temperature is higher.

It can be concluded that the effect of temperature overcomes that of composition (Fig. 17). Thus, ideal voltage (Fig. 17) is higher where temperature is higher (Fig. 16) despite a delay in the cross point of voltage lines with respect to temperature lines which take place at 50 and 80 cm from the entrance to the cell, respectively. This delay is caused by the effect of gas composition, whose influence opposes that of temperature.

10. Conclusions

The potential and reliability of the model developed has been shown. This computational tool includes a very detailed electrochemical model of performance, which is the result of a complete analysis of previous works and includes new approaches to critical tasks such as internal reforming of natural gas. In this case, reaction equilibrium and kinetics have been considered.

The simulation of heat transfer phenomena inside the cell has been done in a very careful way so that no information about local heat flows and/or temperatures were lost or neglected. For this purpose, radiation between anodic gas and surface has been considered.

Particular conclusions are listed below:

1. The effect of anodic gas radiation can be neglected under normal operating conditions. However, results should be lowered by 1% if fuel flow increases considerably, this situation being related to high current density and pressure and low fuel utilization factor.
2. The behaviour of the reforming reaction is not uniform along the cell. Care should be taken when considering whether equilibrium is reached or not, specially when methane con-

centration drops down and temperature increases. These conditions are usually found at the second half of the cell.

3. The model presented applies to cells in the inner part of the stack but a fully three-dimensional study must be done in order to evaluate the influence of peripheral cells on the global performance of the stack.

It can be concluded that the tool presented can help to develop tubular solid oxide fuel cell technology, improving both cell performance and reliability. Multidimensional models are essential to fuel cell researchers and manufacturers as long as installation costs are still very high and research cannot rely on tests entirely.

References

[1] S. Campanari, P. Iora, Definition and sensitivity analysis of a finite volume SOFC model for a tubular cell geometry, J. Power Sources 132 (2004) 113–126.

[2] J. Meusinger, E. Riensche, U. Stimming, Reforming of natural gas in solid oxide fuel cell systems, J. Power Sources 71 (1998) 315–320.

[3] U.G. Bossel, Final Report on SOFC Data Facts and Figures, Swiss Federal Office of Energy, Berne, 1992.

[4] A.L. Dicks, Advances in catalysts for internal reforming in high temperature fuel cells, J. Power Sources 71 (1998) 111–122.

[5] Fuel Cell Handbook, 5th ed., U.S. Department of Energy, Morgantown, 2000.

[6] A.F. Massardo, F. Lubelli, Internal reforming solid oxide fuel cell-gas turbine combined cycles (IRSOFC-GT). Part I. Cell model and cycle thermodynamic analysis, J. Eng. Gas Turbines Power 122 (2000) 27–35.

[7] A. Selimovic, Modelling of solid oxide fuel cells applied to the analysis of integrated systems with gas turbine, Doctoral Thesis, University of Lund, Lund, 2002.

[8] R. Peters, E. Riensche, P. Cremer, Pre-reforming of natural gas in solid oxide fuel-cell systems, J. Power Sources 86 (2000) 432–441.

[9] C. Stiller, B. Thorud, S. Seljebo, O. Mathisen, H. Karoliussen, O. Bolland, Finite-volume modelling and hybrid-cycle performance of planar and tubular solid oxide fuel cells, J. Power Sources 141 (2005) 227–240.

[10] C. Haynes, Simulation of tubular solid oxide fuel cell behavior for integration into gas turbine cycles, PhD Thesis, Georgia Institute of Technology, Atlanta, 1999.

[11] K. Ahmed, K. Fogger, Kinetics of internal steam reforming of methane on Ni/YSZ-based anodes for solid oxide fuel cells, Catal. Today 63 (2000) 479–487.

[12] L. Magistri, R. Bozzo, P. Costamagna, A.F. Massardo, Simplified versus detailed solid oxide fuel cell reactor models and influence on the simulation of the design point performance of hybrid systems, J. Eng. Gas Turbines Power 126 (2004) 516–523.

[13] T. Ota, M. Koyama, C. Wen, K. Yamada, H. Takahashi, Object-based modelling of SOFC system: dynamic behaviour of micro-tube SOFC, J. Power Sources 118 (2003) 430–439.

[14] H. Wendt, G. Kreysa, Electrochemical Engineering, Springer, Berlin, 1999.

[15] P. Costamagna, K. Honegger, Modelling of solid oxide heat exchanger integrated stacks and simulation at high fuel utilization, J. Electrochem. Soc. 145 (11) (1998) 3995–4006.

[16] S.H. Chan, K.A. Kohr, Z.T. Xia, A complete polarization model of a solid oxide fuel cell and its sensitivity to the change of cell component thickness, J. Power Sources 93 (2001) 130–140.

[17] K. Nisancioglu, Ohmic losses, in: Proceedings of the IEA Workshop on Mathematical Modelling, Charmey, 1998, pp. 87–98.

[18] B. Todd, J.B. Young, Thermodynamic and transport properties of gases for use in solid oxide fuel cell modelling, J. Power Sources 110 (2002) 186–200.

[19] D. Sánchez, Aportación al análisis de pilas de combustible de óxido sólido (SOFC) para integración en sistemas híbridos pila de combustible-turbina de gas, Tesis Doctoral, Universidad de Sevilla, Sevilla, 2005 (in Spanish).

[20] W.M. Rohsenhow, J. Hartnett, E. Ganic, Handbook of Heat Transfer Fundamentals, 2nd ed., McGraw Hill, New York, 1973.

[21] H.D. Baehr, K. Stephan, Heat and Mass Transfer, Springer, Berlin, 1998.

[22] S. Nagata, A. Momma, T. Kato, Y. Kasuga, Numerical analysis of output characteristics of tubular SOFC with internal reformer, J. Power Sources 101 (2001) 60–71.

[23] P. Li, M. Chyu, Simulation of the chemical/electrochemical reactions and heat/mass transfer of a tubular SOFC in a stack, J. Power Sources 124 (2003) 487–498.

[24] P. Li, L. Schaefer, M. Chyu, A numerical model coupling the heat and gas species' transport processes in a tubular SOFC, J. Heat Transfer 126 (2004) 219–229.

[25] J.G. Pharoah, J.D.J. Van der Steen, The effect of radiation heat transfer in solid oxide fuel cell modelling, in: Proceedings of the Spring Technical Meeting at Queen's University, 2004.

[26] S. Samuelsen, Analysis and Technology Transfer for Fuel Cell Systems, Pier Project, California Energy Commission, Irvine, 2000.

[27] S. Hadvig, Gas emissivity and absortivity, J. Inst. Fuel 43 (1970) 129–135.

[28] F. Kreith, M.S. Bohn, Principles of Heat Transfer, 4th ed., Harper and Rove, New York, 1986.

[29] N. Brandon, D. Thompsett, Fuel Cells Compendium, Elsevier, Oxford, 2005.

[30] A. Hirano, M. Suzuki, M. Ipponmatsu, Evaluation of a new solid oxide fuel cell system by non-isothermal modelling, J. Electrochem. Soc. 139 (10) (1992) 2744–2751.